JCTC Journal of Chemical Theory and Computation

Article

Cite This: J. Chem. Theory Comput. 2018, 14, 5701−5714

pubs.acs.org/JCTC

Performance and Scope of Perturbative Corrections to Random-Phase Approximation Energies

Guo P. Chen, Matthew M. Agee, and Filipp Furche*

University of California, Irvine, Department of Chemistry, 1102 Natural Sciences II, Irvine, California 92697-2025, United States

Supporting Information

ABSTRACT: It has been suspected since the early days of the random-phase approximation (RPA) that corrections to RPA correlation energies result mostly from short-range correlation effects and are thus amenable to perturbation theory. Here we test this hypothesis by analyzing formal and numerical results for the most common beyond-RPA perturbative corrections, including the bare second-order exchange (SOX), second-order screened exchange (SOSEX), and approximate exchange kernel (AXK) methods. Our analysis is facilitated by efficient and robust algorithms based on the resolution-of-the-identity (RI) approximation and numerical frequency integration, which enable benchmark beyond-RPA calculations on medium- and large-size molecules with size-independent accuracy. The AXK method systematically improves upon RPA, SOX, and SOSEX for reaction barrier heights, reaction energies, and noncovalent interaction energies of main-group compounds. The improved accuracy of AXK compared with SOX and SOSEX is attributed to stronger screening of bare SOX in AXK. For reactions involving transition-metal compounds, particularly 3d transition-metal dimers, the AXK correction is too small and can even have the wrong sign. These observations are rationalized by a measure $\bar{\alpha}$ of the effective coupling strength for beyond-RPA correlation. When the effective coupling strength increases beyond a critical $\bar{\alpha}$ value of approximately 0.5, the RPA errors increase rapidly and perturbative corrections become unreliable. Thus, perturbation theory can systematically correct RPA but only for systems and properties qualitatively well captured by RPA, as indicated by small $\bar{\alpha}$ values.

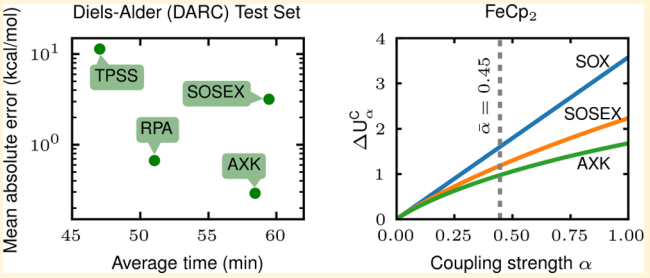

1. INTRODUCTION

Electronic structure methods based on the random-phase approximation (RPA)[1−4] yield consistent accuracy at reasonable computational cost for a wide range of applications in quantum chemistry and solid-state physics. Compared with finite-order perturbation methods, such as second-order Møller−Plesset (MP2) theory,[5] RPA is relatively insensitive to the gap size and free of the divergence problem for metallic systems.[6] RPA captures long-range correlation effects and "seamlessly" accounts for dispersion interactions.[7−9] While RPA takes into account some of the strong correlation arising in dissociating electron pair bonds,[10,11] it has long been recognized that RPA is qualitatively deficient at higher electron coupling strengths and short interaction range,[12,13] as reflected in its inadequate accuracy for ionization and atomization energies.[2]

The formal and computational appeal of RPA has triggered a search for simple remedies to these deficiencies. Corrections based on ground-state density functional theory (DFT),[14,15] including range-separated RPA methods,[16−19] incorporate semilocal density functionals to correct RPA.[20,21] "Local-field corrections" to RPA were pioneered by Singwi, Tosi, Land, and Sjölander (STLS) in the 1960s[12] and may be viewed as an early, physically inspired attempt to devise approximate exchange−correlation (XC) kernels accounting for short-range correlations beyond RPA. Further developments along these lines include the inhomogeneous STLS method,[22] semilocal kernels,[23] local[24] and nonlocal[25,26] energy-optimized kernels, as well as model kernels derived from the uniform electron gas by momentum space cutoff,[27,28] frequency-dependent effective interaction models,[29] and jellium-with-gap models.[30] While these corrections can be designed to deliver high accuracy for certain applications, uniform improvement upon RPA for a wide range of systems and properties at moderate computational cost has been difficult to achieve.

The notion of "beyond-RPA corrections" is based on the implicit assumption that beyond-RPA correlation is, in some sense, small compared with correlation effects captured by RPA. For the uniform electron gas, conventional many-body perturbation theory diverges in every order due to the long range of the *bare* electron−electron Coulomb interaction.[31] On the other hand, the effective interaction accounting for beyond-RPA correlation is shorter ranged, at least for high to intermediate densities,[32] suggesting that perturbation theory may be an effective means to derive beyond-RPA corrections. This led to the development of second-order perturbative

Received: July 27, 2018
Published: September 21, 2018

DOI: 10.1021/acs.jctc.8b00777
J. Chem. Theory Comput. 2018, 14, 5701−5714

corrections to RPA, starting with the second-order screened exchange (SOSEX) method.[13,33,34] Unlike RPA, SOSEX is one-electron self-correlation-free,[35] but it incorrectly dissociates covalent bonds within the spin-restricted formalism[35] and produces less accurate reaction barrier heights than RPA.[36−38] RPA-renormalized many-body perturbation theory is based on a perturbative expansion of the Bethe−Salpeter equation (BSE)[39,40] starting from RPA as the zero-order solution.[38] The second-order RPA-renormalized perturbation method using the approximate exchange kernel (AXK)—hereafter referred to as the AXK method—yielded more accurate energetics than RPA for small molecules, consistently improving upon RPA for ionization and atomization energies.[38] These results also suggested that AXK preserves the accuracy of RPA and outperforms SOSEX for reaction barrier heights. Nevertheless, the lack of efficient implementations has hampered thorough assessment of AXK in the past.

In this paper, we present two AXK algorithms that scale as $O(N^5 \ln N)$ and $O(N^4 \ln N)$ with the system size N. These algorithms also enable efficient SOSEX and bare second-order exchange (SOX) calculations. Low-scaling SOSEX and AXK algorithms have been proposed in refs 38 and 41−46, and a SOSEX implementation with subcubic effective scaling for linear alkanes has been recently reported in ref 46. Our primary aim is to enable efficient calculations for moderately large molecular systems with constant, predetermined accuracy regardless of scaling. This enables critical assessment of second-order beyond-RPA corrections using diverse benchmark sets for reaction barrier heights, reaction energies, and noncovalent interaction energies. We also present tests on dissociation energies of charged dimers where the RPA self-correlation error is pronounced and of transition-metal compounds that feature diverse bondings. Finally, we discuss whether, and under what circumstances, perturbative corrections to RPA are worthwhile.

2. THEORY

2.1. Random-Phase Approximation. Within the zero-temperature adiabatic-connection fluctuation−dissipation (ACFD) DFT framework, the ground-state correlation energy can be expressed as[47,48]

$$E^{\mathrm{C}} = -\frac{1}{2\pi}\int_0^1 \mathrm{d}\alpha\ \mathrm{Re}\int_0^\infty \mathrm{d}\omega\ \langle \mathbf{V}(\mathbf{\Pi}_\alpha(\mathrm{i}\omega) - \mathbf{\Pi}_0(\mathrm{i}\omega))\rangle \tag{1}$$

where

$$\mathbf{V} = \begin{pmatrix} \mathbf{B}^{\mathrm{H}} & \mathbf{B}^{\mathrm{H}} \\ \mathbf{B}^{\mathrm{H}} & \mathbf{B}^{\mathrm{H}} \end{pmatrix} \tag{2}$$

denotes the Hartree interaction between particle−hole (ph) pairs. $B^{\mathrm{H}}_{iajb} = (ialjb)$ is a four-index Coulomb integral in Mulliken notation; indices i, j, ... stand for occupied and a, b, ... for unoccupied spin−orbitals in a spin-unrestricted Kohn−Sham (KS) reference. Brackets denote the trace operation. Orbitals are assumed to be real-valued throughout this paper.

$$\mathbf{\Pi}_0(\mathrm{i}\omega) = -\begin{pmatrix} \mathbf{D} - \mathrm{i}\omega\mathbf{1} & \mathbf{0} \\ \mathbf{0} & \mathbf{D} + \mathrm{i}\omega\mathbf{1} \end{pmatrix}^{-1} \tag{3}$$

is the noninteracting polarization propagator, where $D_{iajb} = (\epsilon_a - \epsilon_i)\delta_{ij}\delta_{ab}$ is a diagonal matrix of KS orbital energy differences. The adiabatic-connection polarization propagator $\mathbf{\Pi}_\alpha$ yields the same density−density response function as the interacting polarization propagator[4] and is related to $\mathbf{\Pi}_0$ through the BSE[40,49]

$$\mathbf{\Pi}_\alpha(\mathrm{i}\omega) = (\mathbf{\Pi}_0(\mathrm{i}\omega)^{-1} - \alpha\mathbf{V} - \mathbf{K}_\alpha(\mathrm{i}\omega))^{-1} \tag{4}$$

where $\mathbf{K}_\alpha(\mathrm{i}\omega)$ is the BSE XC kernel at coupling strength α. Note that this BSE describes the response of the system associated with the adiabatic-connection Hamiltonian[47,50] rather than that of the interacting system. Analytic continuation of the polarization propagators to the upper complex frequency plane has been performed, permitting frequency integration along the imaginary axis.

The RPA, also known as *bare* or *direct* RPA, neglects the XC kernel and only accounts for ph−ph interactions through the Hartree kernel,[31] eq 2; therefore

$$\mathbf{\Pi}^{\mathrm{RPA}}_\alpha(\mathrm{i}\omega) = (\mathbf{\Pi}_0(\mathrm{i}\omega)^{-1} - \alpha\mathbf{V})^{-1} \tag{5}$$

The positive definiteness and symmetry of $\mathbf{B}^{\mathrm{H}}$ warrant a decomposition

$$\mathbf{B}^{\mathrm{H}} = \mathbf{S}\mathbf{S}^{\mathrm{T}} \tag{6}$$

Here the decomposition is full-rank and can be realized using, e.g., the Cholesky factorization. Its low-rank approximation will be presented in section 3.1. We may therefore write

$$\mathbf{V} = \boldsymbol{\eta}\boldsymbol{\eta}^{\mathrm{T}} \tag{7}$$

where

$$\boldsymbol{\eta} = \begin{pmatrix} \mathbf{S} \\ \mathbf{S} \end{pmatrix} \tag{8}$$

Using the Sherman−Morrison−Woodbury formula,[51] the RPA polarization propagator can then be written as

$$\mathbf{\Pi}^{\mathrm{RPA}}_\alpha(\mathrm{i}\omega) = \mathbf{\Pi}_0(\mathrm{i}\omega) + \mathbf{\Pi}_0(\mathrm{i}\omega)\mathbf{W}_{1,\alpha}(\mathrm{i}\omega)\mathbf{\Pi}_0(\mathrm{i}\omega) \tag{9}$$

where

$$\mathbf{W}_{1,\alpha}(\mathrm{i}\omega) = \alpha\boldsymbol{\eta}\boldsymbol{\kappa}_\alpha(\mathrm{i}\omega)^{-1}\boldsymbol{\eta}^{\mathrm{T}} \tag{10}$$

$$\boldsymbol{\kappa}_\alpha(\mathrm{i}\omega) = \mathbf{1} - \alpha\boldsymbol{\eta}^{\mathrm{T}}\mathbf{\Pi}_0(\mathrm{i}\omega)\boldsymbol{\eta} \tag{11}$$

are, respectively, the effective interaction and the generalized dielectric function within RPA. These quantities assume symmetrized forms that facilitate numerical implementations and low-rank approximations, as will be discussed in section 3. Similar definitions in reciprocal space were used in condensed matter computations.[52,53] The effective interaction $\mathbf{W}_{1,\alpha}(\mathrm{i}\omega)$ is the only coupling-strength-dependent quantity in eq 9. Analytic coupling strength integration can be performed for $\mathbf{W}_{1,\alpha}(\mathrm{i}\omega)$, leading to the RPA correlation energy[41,48]

$$E^{\mathrm{C\,RPA}} = \frac{1}{2\pi}\int_0^\infty \mathrm{d}\omega\ \langle \ln(\mathbf{1} + \mathbf{Q}(\omega)) - \mathbf{Q}(\omega)\rangle \tag{12}$$

where we have defined

$$\mathbf{Q}(\omega) = -\boldsymbol{\eta}^{\mathrm{T}}\mathbf{\Pi}_0(\mathrm{i}\omega)\boldsymbol{\eta} = 2\mathbf{S}^{\mathrm{T}}\mathbf{G}(\omega)\mathbf{S} \tag{13}$$

and

$$\mathbf{G}(\omega) = \mathbf{D}(\mathbf{D}^2 + \omega^2\mathbf{1})^{-1} \tag{14}$$

By eqs 11 and 13, $\mathbf{Q}(\omega) = \boldsymbol{\kappa}_\alpha(\mathrm{i}\omega)|_{\alpha=1} - \mathbf{1}$, i.e., $\mathbf{Q}$ is a real-valued matrix function that may be interpreted as a generalized susceptibility accounting for dielectric screening due to induced ph pairs.

DOI: 10.1021/acs.jctc.8b00777
J. Chem. Theory Comput. 2018, 14, 5701−5714

2.2. RPA Renormalization with AXK. The lack of an XC kernel in RPA results in overcorrelation of electrons; bare RPA overestimates the magnitudes of correlation energies by nearly 2-fold. In particular, RPA suffers from self-correlation and leads to unphysical pair density at short electron separations.[12] ph−ph exchange corrections aim to reduce this self-correlation error. Such exchange kernel corrections, however, need to be judiciously constructed to preserve global properties of RPA and avoid degrading the results where RPA is already accurate. For example, the sum of the first-order Hartree and exchange kernels produces instabilities that drastically limit the usefulness of RPA with exchange[54,55] and Hartree−Fock-based RPA.[1,2,10,56,57]

In RPA-renormalized many-body perturbation theory,[38] the adiabatic-connection polarization propagator is expressed in terms of the RPA polarization propagator via

$$\boldsymbol{\Pi}_\alpha(\mathrm{i}\omega) = (\boldsymbol{\Pi}_\alpha^{\mathrm{RPA}}(\mathrm{i}\omega)^{-1} - \mathbf{K}_\alpha(\mathrm{i}\omega))^{-1} \tag{15}$$

The AXK method consists of choosing kernel

$$\mathbf{K}_\alpha^{\mathrm{AXK}} = \alpha\mathbf{K} = \alpha\begin{pmatrix} \mathbf{B}^{\mathrm{X}} & \mathbf{B}^{\mathrm{X}} \\ \mathbf{B}^{\mathrm{X}} & \mathbf{B}^{\mathrm{X}} \end{pmatrix} \tag{16}$$

where $B^{\mathrm{X}}_{iajb} = -(ib|ja)$, and truncating the series expansion of eq 15 with respect to the kernel at first order.[38] The resulting AXK beyond-RPA correlation energy $\Delta E^{\mathrm{C\,AXK}}$ correctly recovers the SOX energy $\Delta E^{\mathrm{C\,SOX}}$ but also contains higher-order terms that amount to screening at higher coupling strength. Using eq 9, we obtain

$$\Delta E^{\mathrm{C\,AXK}} = -\frac{1}{2\pi}\int_0^1 \mathrm{d}\alpha \int_0^\infty \mathrm{d}\omega\, \langle \mathbf{W}_{2,\alpha}(\mathrm{i}\omega)\boldsymbol{\Pi}_0(\mathrm{i}\omega)\mathbf{K}\boldsymbol{\Pi}_0(\mathrm{i}\omega)\rangle \tag{17}$$

$$= -\frac{1}{2\pi}\int_0^\infty \mathrm{d}\omega\, \langle \bar{\mathbf{W}}_2(\mathrm{i}\omega)\boldsymbol{\Pi}_0(\mathrm{i}\omega)\mathbf{K}\boldsymbol{\Pi}_0(\mathrm{i}\omega)\rangle \tag{18}$$

where the effective interaction $\mathbf{W}_{2,\alpha}(\mathrm{i}\omega) = \alpha\boldsymbol{\eta}\boldsymbol{\kappa}_\alpha(\mathrm{i}\omega)^{-2}\boldsymbol{\eta}^{\mathrm{T}}$ is more strongly screened than the RPA effective interaction $\mathbf{W}_{1,\alpha}(\mathrm{i}\omega)$ defined in eq 10. $\bar{\mathbf{W}}_2$, the coupling strength average of $\mathbf{W}_{2,\alpha}$[42] can be integrated analytically[25,38,46]

$$\bar{\mathbf{W}}_2(\mathrm{i}\omega) = \int_0^1 \mathrm{d}\alpha\, \mathbf{W}_{2,\alpha}(\mathrm{i}\omega) = \boldsymbol{\eta} f_2(\mathbf{Q}(\omega))\boldsymbol{\eta}^{\mathrm{T}} \tag{19}$$

where the function f_2 is defined on $[0, \infty)$ according to Table 1. We may rearrange eq 18 and write

$$\Delta E^{\mathrm{C\,AXK}} = -\frac{1}{2\pi}\int_0^\infty \mathrm{d}\omega\, \langle \mathbf{P}_2(\omega)\mathbf{B}^{\mathrm{X}}\rangle \tag{20}$$

where

$$\mathbf{P}_2(\omega) = 4\mathbf{G}(\omega)\mathbf{S}f_2(\mathbf{Q}(\omega))\mathbf{S}^{\mathrm{T}}\mathbf{G}(\omega) \tag{21}$$

$\mathbf{P}_2(\omega)$ is positive semidefinite due to the positive semidefiniteness of $\mathbf{Q}(\omega)$ and the positivity of the function f_2. As a result, $\Delta E^{\mathrm{C\,AXK}}$ is always positive, mitigating the overcorrelation problem of RPA. $-\frac{1}{\pi}\int_0^\infty \mathrm{d}\omega\, \mathbf{P}_2(\omega)$ is an exchange-type correction to the coupling-strength-averaged two-electron reduced density matrix (2RDM); it diminishes the 2RDM and therefore the pair density when ph pairs interact through exchange. As a result, self-correlation of same-spin electrons is removed exactly to second order and approximately to higher orders in the correlation energy.[38]

Similarly, the SOX and SOSEX beyond-RPA correlation energies within the ACFD theorem can be cast into the forms of eqs 17, 18, and 20,[42] with altered effective interactions labeled by subscripts 0 and 1, respectively. Analytic coupling strength integration can also be performed.[41,43] The corresponding $\mathbf{W}_\alpha$, $\bar{\mathbf{W}}$, and f are defined in Table 1. The f functions are plotted in Figure 1. It is readily shown that the AXK beyond-RPA correlation correction is always lower than the SOSEX correction, which is in turn lower than the SOX correction.

Table 1. Definitions of the Effective Interaction $\mathbf{W}_\alpha$ and the Function f for Different Second-Order beyond-RPA Methods

method	subscript	$\mathbf{W}_\alpha(\mathrm{i}\omega)$	$f(x)$
SOX	0	$\alpha\mathbf{V} = \alpha\boldsymbol{\eta}\boldsymbol{\eta}^{\mathrm{T}}$	$1/2$
SOSEX	1	$\alpha\boldsymbol{\eta}\boldsymbol{\kappa}_\alpha(\mathrm{i}\omega)^{-1}\boldsymbol{\eta}^{\mathrm{T}}$	$-x^{-2}\ln(1+x) + x^{-1}$
AXK	2	$\alpha\boldsymbol{\eta}\boldsymbol{\kappa}_\alpha(\mathrm{i}\omega)^{-2}\boldsymbol{\eta}^{\mathrm{T}}$	$x^{-2}\ln(1+x) - x^{-1}(1+x)^{-1}$

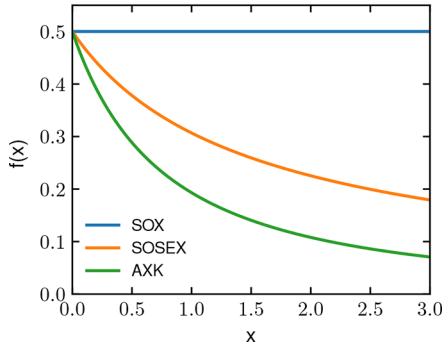

Figure 1. Function specifying the coupling-strength-averaged effective interaction for a beyond-RPA exchange correction method; see Table 1.

For each method, f is a function of $\mathbf{Q}(\omega)$ and characterizes the coupling-strength-averaged effective interaction due to screening. As shown in Figure 1, the AXK f_2 function decays more rapidly than its SOSEX and SOX counterparts. Because the SOSEX effective interaction $\mathbf{W}_{1,\alpha}(\mathrm{i}\omega)$ is identical to that of RPA, the AXK screening is stronger than the RPA screening, particularly for large eigenvalues of $\mathbf{Q}(\omega)$. For the uniform electron gas with high density, large eigenvalues of $\mathbf{Q}(\omega)$ originate from small momentum transfers,[58,59] which correspond to long-range interelectron distances; therefore, the AXK correction to the pair density in the long-range region is strongly attenuated, and its main effects are in the short-range region. This is consistent with the observation that beyond-RPA correlation in the uniform electron gas is short-ranged at high and intermediate densities.[48,59,60]

3. IMPLEMENTATIONS

3.1. RI Approximation. The resolution-of-the-identity (RI) approximation[61,62] provides a low-rank approximation of $\mathbf{B}^{\mathrm{H}}$ by introducing an auxiliary basis set of N_{aux} atom-centered Gaussian functions labeled by P, Q, ... and setting $S_{iaP} = \sum_Q (ia|Q)[\mathbf{L}^{-1}]_{QP}$ in eq 6, where $(ia|Q)$ is a three-index Coulomb integral and $\mathbf{L}$ is the Cholesky factor of the $N_{\mathrm{aux}} \times N_{\mathrm{aux}}$ matrix of two-index Coulomb integrals $(P|Q)$. N_{aux} scales only linearly with the system size N. In the following, the RI approximation for $\mathbf{S}$ is assumed unless stated otherwise. A key property of RI-RPA is that the RI-RPA correlation energy is variationally bounded from below by the RPA correlation energy obtained without RI.[41] A formal proof of this property

DOI: 10.1021/acs.jctc.8b00777
J. Chem. Theory Comput. 2018, 14, 5701−5714

assuming weaker conditions than those of the prior work is provided in the Appendix. The RI approximation is also referred to as density fitting in the Coulomb metric. While density fitting methods in local metrics may lead to more favorable scaling,[63−65] their lack of variational stability can give rise to larger errors.[62,64,65] Schemes to recover[66] or partially recover[67] variational stability for density fitting in local metrics are still under active development.

3.2. Molecular Orbital Based AXK Algorithm. A straightforward evaluation of the integrand of eq 20 scales as $O(N^6)$ because all of the matrices therein are $N_h N_p \times N_h N_p$, where N_h and N_p denote the numbers of occupied and virtual orbitals, respectively. The scaling is reduced to $O(N^5)$ with the RI approximation because $\Delta E^{C\,AXK}$ may be expressed in terms of matrices that either scale as N^2 or N^3 or may be computed on the fly.

With RI, the dimension of the $\mathbf{Q}(\omega)$ matrix defined in eq 13 is $N_{aux} \times N_{aux}$ and scales quadratically with N. An eigen decomposition of $\mathbf{Q}(\omega)$ can be readily performed with $O(N^3)$ operations, yielding

$$\mathbf{Q}(\omega) = \mathbf{X}(\omega)\mathbf{q}(\omega)\mathbf{X}^T(\omega) \tag{22}$$

A symmetric decomposition $\mathbf{P}_2(\omega) = \mathbf{R}(\omega)\mathbf{R}^T(\omega)$ thereby follows, where

$$\mathbf{R}(\omega) = 2\mathbf{G}(\omega)\mathbf{S}\mathbf{X}(\omega)(f_2(\mathbf{q}(\omega)))^{1/2} \tag{23}$$

is an $N_h N_p \times N_{aux}$ matrix. For a given ω, $\mathbf{R}(\omega)$ and $\mathbf{P}_2(\omega)$ can be constructed with $O(N^4)$ and $O(N^5)$ operations, respectively. We drop the subscript 2 in the following because the same algorithm can also be applied to SOX and SOSEX.

The frequency integration can be performed using the same Clenshaw−Curtis quadrature as in the RI-RPA algorithm,[41] with quadrature points and weights denoted as $\{\omega_I\}$ and $\{w_I\}$, respectively, where $I = 1,...,N_g$. Because the integration is mapped to an equidistant quadrature on the interval $[0, \pi/2]$, a nested quadrature rule can be designed. The error of the Clenshaw−Curtis quadrature decreases exponentially with N_g.[68] Therefore, an extra $O(\ln N)$ scaling factor arises if size-independent accuracy is desired.

Straightforward application of the RI approximation to $\mathbf{B}^X$ leads to $O(N^5 \ln N)$ scaling, as outlined in Algorithm 1 in the Supporting Information (SI). This algorithm is easily parallelized using shared-memory parallel basic linear algebra subprograms (BLAS).[69] The frequency integration loop is kept outermost to facilitate future implementations of hierarchical distributed-memory parallelism. The higher asymptotic scaling of this algorithm compared with that of RI-RPA reflects the well-known result that RI methods are significantly less efficient for exchange-type contractions than for direct-type contractions.

3.3. Atomic Orbital Based AXK Algorithm. The scaling of evaluating $\Delta E^{C\,AXK}$ can be further reduced if the exchange-type contraction in eq 20 is computed using integral-direct techniques.[70] This requires transformation of $\mathbf{R}(\omega)$, and therefore $\mathbf{P}(\omega)$, to the atomic orbital (AO) basis according to

$$R_{\lambda\mu P}(\omega) = \sum_{ia} C_{\lambda i} C_{\mu a} R_{iaP}(\omega) \tag{24}$$

where $\mathbf{C}$ is the orbital coefficient matrix; Greek indices denote AO basis functions. We use the same symbol for quantities in the molecule orbital (MO) and AO representations; they can be distinguished by the set of indices being used. The AXK correction is obtained by contracting the AO exchange integrals with the transformed $\mathbf{P}$, i.e.

$$\Delta E^{C\,AXK} = \frac{1}{2\pi}\int_0^\infty d\omega \sum_{\kappa\lambda\mu\nu} P_{\lambda\mu\nu\kappa}(\omega)(\kappa\lambda|\mu\nu) \tag{25}$$

Both $\mathbf{P}$ and the integrals are prescreened using the Cauchy−Schwarz inequality.[71] However, the screening is mainly due to the sparsity of the integrals; the sparsity of $\mathbf{P}$ is not prominent, as opposed to constructing the exchange part of the Fock matrix, in which sparsity is enhanced by the difference density matrix technique.[71] As a result, the scaling of integral computation is $O(N^2)$, and the construction of $\mathbf{R}(\omega)$ and $\mathbf{P}(\omega)$ requires $O(N^4)$ and $O(N^3)$ operations, respectively, for a given ω. The algorithm, outlined in Algorithm 2 in the SI, scales as $O(N^4 \ln N)$ after numerical frequency integration. The algorithm is parallelized over the κ and λ loops using OpenMP.[72] Again, the numerical frequency integration loop is outermost to enable further parallelism over distributed quadrature points and to facilitate more effective screening for each frequency quadrature point.

4. COMPUTATIONAL DETAILS

Both the MO and AO based AXK algorithms were implemented in the `rirpa` module of the TURBOMOLE quantum chemistry program package[73] and are scheduled for a future public release. The SOX and SOSEX beyond-RPA methods were implemented similarly according to section 2.2. All reference KS calculations were performed in C_1 point group symmetry using the Tao−Perdew−Staroverov−Scuseria (TPSS) meta-generalized gradient approximation (meta-GGA) functional,[74] which has been shown to yield uniform accuracy even for transition-metal compounds.[75,76] For the KS calculations, density matrix and energy convergence criteria were set to 10^{-7} or tighter, and fine density grids of at least m5 quality[77] were used. Core electrons were kept frozen in RPA-type calculations. Coupling-strength-dependent AXK and SOSEX calculations without the RI approximation were performed using the `mpgrad` module in TURBOMOLE 7.2.[38]

Karlsruhe def2-series basis sets of double-ζ (SVP), triple-ζ (TZVP), and quadruple-ζ (QZVPP) quality were used.[78,79] The corresponding auxiliary basis sets optimized for RI-MP2[80,81] were used for the RI approximation in the RPA and beyond-RPA calculations. For validation, the complete basis set (CBS) limit of the correlation energy $E^C(\infty)$ is estimated using the two-point extrapolation scheme[82,83]

$$E^C(X) = E^C(\infty) + A/X^3 \tag{26}$$

where X is the cardinal number of the basis set and A is a coefficient to be determined. The correlation-consistent basis sets aug-cc-pVXZ (AVXZ; X = T, Q, 5)[84−86] and corresponding auxiliary basis sets[81,87,88] were used for the basis set extrapolation calculations. For all of the correlation energy calculations using the AVXZ basis sets, the KS energy expectation values were computed using the QZVPP basis set, which yields small basis set superposition errors.[78]

5. RESULTS

In this section, we first validate our implementations by estimating the errors due to integral prescreening, the RI approximation, and numerical frequency integration. Timings

DOI: 10.1021/acs.jctc.8b00777
J. Chem. Theory Comput. 2018, 14, 5701−5714

of the algorithms are measured using large mesityl-substituted porphyrin molecules[89] as well as benchmark sets from the GMTKN55 database for diverse reaction barrier heights (BHDIV10), Diels–Alder reaction energies (DARC), and interaction energies of *n*-alkane dimers (ADIM6).[90,91] We then test the accuracy of the AXK methods using these benchmarks as well as a benchmark set for assessing the self-interaction error (SIE4x4)[90,91] and a 3d transition-metal reference set proposed in ref 76. These benchmark systems contain diverse types of molecules and bonding situations featuring weak to moderately strong correlations.

5.1. Integral Prescreening. In the AO based algorithm, the integral prescreening is performed according to

$$\frac{1}{2\pi} w_I (P_{\lambda\mu\lambda\mu}(\omega_I) P_{\nu\kappa\nu\kappa}(\omega_I) (\kappa\lambda|\kappa\lambda)(\mu\nu|\mu\nu))^{1/2} \leq \frac{\varepsilon}{N_g \sqrt{N_{bf}}} \tag{27}$$

for a shell quadruple κ, λ, μ, ν at a frequency point ω_I. Here, ε is the screening threshold, and N_{bf} is the number of basis functions. The $1/N_g$ factor guarantees that the screening error does not increase with the number of quadrature points. The $1/\sqrt{N_{bf}}$ factor is included to make the screening error size-independent, assuming that entries screened by eq 27 are independent and mean zero.[92] This is opposed to the recent low-scaling SOSEX implementation,[46] where a constant screening threshold was used for all systems. Table 2 summarizes the integral screening errors with various screening thresholds for $\Delta E^{C\ AXK}$ of molecules in the DARC benchmark set. $\varepsilon = 10^{-7}$ is chosen for all of the following AO based beyond-RPA calculations.

Table 2. Mean Errors (ME) and Maximum Absolute Errors (MXE) of $\Delta E^{C\ AXK}$ (in E_h) due to Integral Screening for Compounds in the DARC Benchmark Set[93,94] Relative to Values Obtained with $\varepsilon = 10^{-10}$[a]

ε	10^{-6}	10^{-7}	10^{-8}	10^{-9}
ME	-2.9×10^{-4}	-2.4×10^{-5}	-1.6×10^{-6}	-8.5×10^{-8}
MXE	5.0×10^{-4}	4.2×10^{-5}	2.9×10^{-6}	1.6×10^{-7}

[a]The TZVP basis set was used.

5.2. Accuracy of the RI Approximation. Two kinds of RI approximation errors arise in the present implementations. The first originates from the RI approximation of the Hartree kernel in RPA. This kind of RI error is assumed to be similar to that in the RI-RPA algorithm, where the error is bounded thanks to the variational boundedness of $\mathbf{Q}(\omega)$ within the RI approximation (see the Appendix). Here we assess the second kind of RI error, which only exists in the MO based algorithm and is due to the RI approximation of $\mathbf{B}^X$. It is readily shown that this kind of RI approximation is variational and errors are always negative. Table 3 summarizes the RI errors of the second kind for molecules in the BHDIV10, DARC, and ADIM6 benchmark sets.[90] The errors are on the order of 100 μE_h for all of these systems.

5.3. Accuracy of the Quadrature. Figure 2 shows the numerical integration errors in AXK beyond-RPA correlation energies for molecules in the DARC benchmark set[93,94] and the 3d transition-metal reference set.[76] The transition-metal reference set contains small-gap open-shell species, which demand large numbers of quadrature points.[41] These results were obtained using the MO based algorithm. For both sets of molecules, the errors decrease rapidly with increasing number of quadrature points. Particularly, the exponential decay of the error is observed for the DARC benchmark set with the QZVPP basis set. Moreover, the numerical integration errors for $\Delta E^{C\ AXK}$ are almost always positive, whereas the numerical integration errors for $E^{C\ RPA}$ are almost always negative. The errors in the total correlation energies are on the same order as the errors in $\Delta E^{C\ AXK}$. Generally, a quadrature with 100 points leads to sub-mE_h error due to numerical integration. For energy differences, smaller quadratures may be used because of error cancellation. A nested Clenshaw–Curtis rule doubling N_g until a predetermined precision is achieved was also implemented. For benchmark purposes, very fine frequency quadratures with 400 points were used unless otherwise stated.

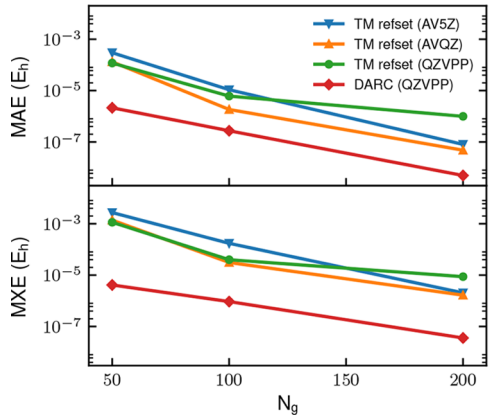

Figure 2. Mean absolute errors (MAE) and maximum absolute errors (MXE) of $\Delta E^{C\ AXK}$ due to the numerical frequency integration with varying number of quadrature points N_g for the transition-metal reference set (TM refset)[76] and the DARC benchmark set,[93,94] using the QZVPP, AVQZ, and AV5Z basis sets. Reference values were obtained from calculations with fine quadratures of $N_g = 400$.

5.4. Performance. We assess the performance of our implementations using all of the molecules in the BHDIV10, DARC, and ADIM6 benchmarks from the GMTKN55 database[90] using different basis sets. We also carried out AXK calculations for mesityl-substituted porphyrin monomer and dimer[89] with 113 and 224 atoms, respectively, using the

Table 3. Mean Errors (ME) and Maximum Absolute Errors (MXE) of $\Delta E^{C\ AXK}$ (in E_h) due to the RI Approximation of the Exchange Integrals[a]

	BHDIV10		DARC		ADIM6	
	SVP	TZVP	SVP	TZVP	SVP	TZVP
ME	-3.6×10^{-4}	-1.9×10^{-4}	-5.2×10^{-4}	-2.6×10^{-4}	-4.0×10^{-4}	-2.2×10^{-4}
MXE	6.7×10^{-4}	3.5×10^{-4}	8.3×10^{-4}	4.3×10^{-4}	8.4×10^{-4}	4.6×10^{-4}

[a]Calculations were performed for all of the species in the BHDIV10, DARC, and ADIM6 benchmark sets[90] using the SVP and TZVP basis sets.

DOI: 10.1021/acs.jctc.8b00777
J. Chem. Theory Comput. 2018, 14, 5701–5714

SVP basis set. The timing results are shown in Figure 3, wherein the effective scalings are also listed. Clearly, the

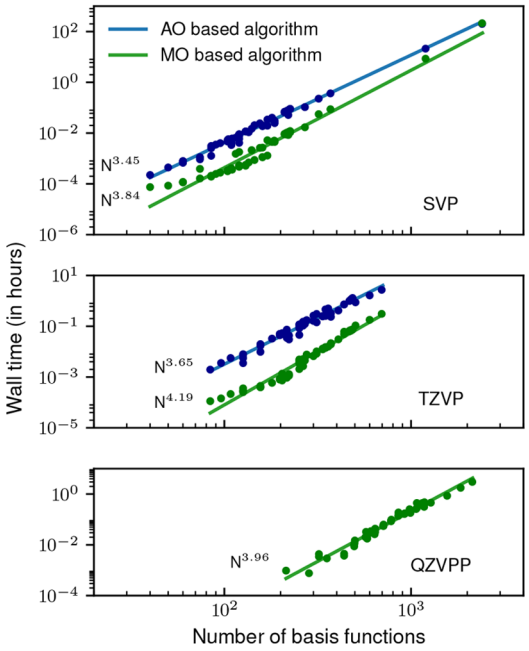

Figure 3. Timing results for AXK total energy calculations on molecules in the BHDIV10, DARC, and ADIM6 benchmark sets[90] as well as mesityl-substituted porphyrins[89] (SVP only) using the SVP, TZVP, and QZVPP basis sets. The effective scalings are listed next to the fitted lines. The timings were done for calculations with $N_g = 50$. All calculations were performed on a 20-core Intel Xeon E5-2680 2.80 GHz workstation using a maximum of 80 GiB of memory.

asymptotic quintic and quartic scalings do not show up for these test calculations yet. Although the AO based algorithm scales more favorably, it is less efficient for most of the small- and medium-size molecules due to a large scaling prefactor. The AO based algorithm eventually becomes faster than the MO based algorithm for the large mesityl-substituted porphyrin dimer with the SVP basis set; see Table 4. However, for calculations with quadruple-ζ basis sets, the AO based algorithm is impractical because the prefactor becomes larger due to inefficient integral screening.

Table 4. Timing Results[a] for the Mesityl-Substituted Porphyrin Monomer ($NiC_{56}H_{52}N_4$) and Dimer ($Ni_2C_{112}H_{100}N_{10}$)[89,b]

system	N_{bf}	t^{MO}	t^{AO}
$NiC_{56}H_{52}N_4$	1196	8.53	21.20
$Ni_2C_{112}H_{100}N_{10}$	2402	212.45	200.04

[a]The timing results are wall time in hours. [b]The calculations were performed on a 20-core Intel Xeon E5-2680 2.80 GHz workstation using a maximum of 80 GiB of memory.

As we shall see in the following benchmark calculations, basis sets of at least triple-ζ quality need to be used for accurate AXK energetics. For this reason, the following benchmark calculations were performed using the MO based algorithm.

5.5. Benchmarks. *5.5.1. Reaction Barrier Heights.* Accurate prediction of reaction barrier heights requires a balanced treatment of static correlation and self-interaction.[95,96] Semilocal DFT generally underestimates barrier heights,[97] whereas single-reference perturbation methods are prone to overestimation.[98,99] Here we present benchmark calculations for the BHDIV10 set,[90] which contains 10 reactions of medium-size molecules and features diverse barrier heights ranging from 13.64 to 96.17 kcal/mol. Results obtained using the QZVPP basis set are shown in Table 5.

As expected, the TPSS meta-GGA functional underestimates the BHDIV10 barrier heights, except for reaction 2, which is the isomerization from 1,4-azaborine to B−N Dewar benzene. Adding the D3 dispersion correction[100] does not improve the results, indicating that the dispersion interaction energy does not change much from the reactants to the transition states. The RPA barrier heights are significantly more accurate, yet they are still statistically slightly lower than the reference values. Compared with RPA, AXK systematically increases the calculated barrier heights and further reduces the mean absolute error (MAE) from 1.64 to 1.30 kcal/mol. SOSEX yields even larger barrier heights and overcorrects RPA, especially for reactions that break π bonds (reactions 2, 4, and 8). These results are consistent with previous tests on small-molecule reactions.[38] The barrier heights from the bare SOX correction are too high, as expected from the reduced KS gaps of transition states relative to those of the reactants. The poor accuracy of bare SOX reflects the fact that the SOX coupling strength dependence is linear (see Table 1); thus, bare SOX works for only very weakly correlated systems such as the uniform electron gas in the high-density limit or weak interactions of closed-shell systems at large separation but falls short even for the slightly stronger correlations present in the transition states in our test calculations.

More extensive tests using different basis sets are summarized in Table S1. The basis set convergence for RPA and AXK is significantly slower than that for semilocal DFT; as a result, basis sets of at least triple-ζ quality are required to make an AXK calculation of energy differences worthwhile.

5.5.2. Diels−Alder Reaction Energies. A Diels−Alder (DA) reaction is an example of pericyclic reactions and involves concertedly breaking and forming π and σ bonds. Semilocal DFT predicts DA reaction energies that are less exothermic than those of explicitly correlated coupled-cluster calculations at the CBS limit.[90,93] It has been suggested that the errors are due to self-interaction[93] and intramolecular dispersion interactions.[101] RPA has been shown to be quite accurate for DA reaction energies; however, the RPA+ short-range semilocal correction method[15] and SOSEX lead to systematic over- and underestimation, respectively.[101]

In Table 6, we present reaction energy calculations on a set of 14 DA reactions (the DARC benchmark).[93,94] Table S2 summarizes the results obtained using different basis sets. We note in passing that basis sets of at least triple-ζ quality are necessary for RPA-type calculations. As with the results in ref 93, semilocal DFT calculations with the TPSS functional overestimate the DA reaction energies. The description of dispersion interactions is indeed important, as indicated by the TPSS calculations with the D3 dispersion correction. The RPA reaction energies are within chemical accuracy, reflecting that RPA adequately accounts for dispersion interactions and reduces self-interaction error through the exact first-order exchange. Nevertheless, RPA slightly underestimates energies of the reactions that yield bicyclic and tricyclic products with close-lying bridgehead carbons (reactions 3, 4, and 7−14) while overestimating the others. AXK almost uniformly

DOI: 10.1021/acs.jctc.8b00777
J. Chem. Theory Comput. 2018, 14, 5701−5714

Table 5. Errors of Calculated Reaction Barrier Heights in kcal/mol Using the QZVPP Basis Set for the BHDIV10 Benchmark Set Relative to Explicitly Correlated Coupled-Cluster Results in Reference 90[a]

reaction	ref	TPSS	TPSS-D3	RPA	AXK	SOSEX	SOX
1	25.65	−10.11	−10.37	−2.33	−0.75	1.69	10.05
2	56.90	1.37	0.94	−1.40	0.84	4.27	14.38
3	36.53	−7.82	−7.21	−1.32	−0.43	1.13	5.54
4	96.17	−6.64	−7.51	−1.24	0.64	3.61	13.47
5	15.94	−7.00	−7.23	0.52	0.92	1.22	2.46
6	13.64	−4.39	−4.84	1.79	2.21	2.09	1.74
7	27.49	−2.73	−3.16	−0.18	0.91	1.71	3.77
8	50.24	−10.12	−10.29	2.88	3.38	3.59	3.88
9	65.84	−7.17	−7.19	−1.49	−0.40	1.11	5.12
10	64.93	−3.41	−3.37	−3.29	−2.50	−1.90	−3.32
ME		−5.80	−6.02	−0.61	0.48	1.85	5.71
MAE		6.08	6.21	1.64	1.30	2.23	6.37
MXE		10.12	10.37	3.29	3.38	4.27	14.38

[a]The structures of the reactants and transition states are provided in ref 91.

Table 6. Errors of Calculated Reaction Energies in kcal/mol Using the QZVPP Basis Set for the DARC Benchmark Set[93,94] Relative to Explicitly Correlated Coupled-Cluster Results from Reference 90[a]

	reaction	ref	TPSS	TPSS-D3	RPA	AXK	SOSEX	SOX
1	ethene + butadiene	−45.4	9.23	6.22	0.91	0.31	−4.83	−22.07
2	ethyne + butadiene	−60.8	4.66	2.88	1.06	0.05	−4.88	−22.32
3	ethene + cyclopentadiene	−29.9	9.49	5.96	−0.24	0.33	−3.12	−15.24
4	ethyne + cyclopentadiene	−33.6	5.00	2.69	−0.73	−0.03	−2.51	−12.23
5	ethene +1,3-cyclohexadiene	−37.6	10.64	6.55	0.30	0.42	−3.78	−18.12
6	ethyne +1,3-cyclohexadiene	−49.0	5.90	3.07	0.35	0.07	−3.85	−17.74
7	furane + maleic anhydride (endo)	−14.0	14.36	8.98	−0.96	0.52	−1.58	−10.53
8	furane + maleic anhydride (exo)	−15.9	14.32	9.28	−0.79	0.47	−1.82	−11.25
9	furane + maleimide (endo)	−16.8	14.47	8.97	−0.78	0.56	−1.87	−12.06
10	furane + maleimide (exo)	−18.9	14.28	9.11	−0.53	0.60	−1.99	−12.58
11	cyclopentadiene + maleic anhydride (endo)	−31.7	14.40	8.52	−0.92	0.01	−3.52	−16.77
12	cyclopentadiene + maleic anhydirde (exo)	−32.2	14.05	8.26	−0.70	0.18	−3.35	−16.53
13	cyclopentadiene + maleimide (endo)	−34.2	14.47	8.46	−0.65	0.13	−3.72	−18.23
14	cyclopentadiene + maleimide (exo)	−34.6	14.10	8.22	−0.42	0.30	−3.56	−17.99
ME			11.38	6.94	−0.29	0.28	−3.17	−15.98
MAE			11.38	6.94	0.67	0.29	3.17	15.98
MXE			14.47	9.28	1.06	0.60	4.88	22.32

[a]For reactions 7−14, the products can be of endo or exo form, as indicated in parentheses.

Table 7. Errors of Calculated Noncovalent Interaction Energies in kcal/mol Using the QZVPP Basis Set and 3-4 Extrapolated Complete Basis Set (CBS) Limit for *n*-Alkane Dimers in the ADIM6 Benchmark Set[100] Relative to Explicitly Correlated Coupled-Cluster Results in Reference 90

		TPSS	TPSS-D3	RPA		AXK		SOSEX		SOX
dimer	ref	QZVPP	QZVPP	QZVPP	CBS	QZVPP	CBS	QZVPP	CBS	QZVPP
$(C_2H_6)_2$	1.34	−1.76	0.22	−0.31	−0.33	−0.27	−0.28	−0.29	−0.28	−0.38
$(C_3H_8)_2$	1.99	−2.71	0.27	−0.37	−0.51	−0.33	−0.42	−0.36	−0.43	−0.51
$(C_4H_{10})_2$	2.89	−4.03	0.38	−0.50	−0.73	−0.46	−0.61	−0.50	−0.62	−0.72
$(C_5H_{12})_2$	3.78	−5.32	0.41	−0.63	−0.95	−0.57	−0.79	−0.63	−0.79	−0.91
$(C_6H_{14})_2$	4.60	−6.59	0.56	−0.68	−1.11	−0.62	−0.92	−0.69	−0.92	−1.05
$(C_7H_{16})_2$	5.55	−8.05	0.40	−0.80	−1.34	−0.73	−1.10	−0.80	−1.09	−1.21
ME		−4.75	0.37	−0.55	−0.83	−0.50	−0.69	−0.54	−0.69	−0.79
MAE		4.75	0.37	0.55	0.83	0.50	0.69	0.54	0.69	0.79
MXE		8.05	0.56	0.80	1.34	0.73	1.10	0.80	1.09	1.21

improves upon RPA, reducing the MAE from 0.67 kcal/mol of RPA to 0.29 kcal/mol. The AXK errors are positive, except for reaction 4, for which the AXK error is almost zero. SOSEX, on the other hand, worsens the RPA reaction energies, leading to appreciable negative errors. The SOSEX results are in line with ref 101, wherein only the first four reactions in the DARC benchmark set were investigated. Bare SOX dramatically underestimates the reaction energies, thus providing another example of the inadequacy of low-order perturbation theory for pericyclic reactions.[102] The trends of SOSEX and SOX errors

DOI: 10.1021/acs.jctc.8b00777
J. Chem. Theory Comput. 2018, 14, 5701−5714

Table 8. Errors of Calculated Dissociation Energies in kcal/mol Using the QZVPP Basis Set for Positively Charged Dimers in the SIE4x4 Benchmark Set[90,a]

d_{MM}/d^0_{MM}	ref	TPSS	TPSS-D3	RPA	AXK	SOSEX	SOX
$(H\cdots H)^+$							
1.00	64.4	4.82	4.82	3.42	0.83	−0.48	−2.56
1.25	58.9	7.81	7.81	4.99	1.75	−0.92	−5.60
1.50	48.7	11.23	11.24	8.22	3.71	−1.48	−12.08
1.75	38.3	14.91	14.95	15.75	9.11	−2.25	−33.41
$(He\cdots He)^+$							
1.00	56.9	25.53	25.53	14.49	5.70	−3.30	−21.99
1.25	46.9	32.40	32.41	26.39	13.96	−6.64	−66.59
1.50	31.3	40.39	40.45	41.83	27.94	−9.91	−181.69
1.75	19.1	48.28	48.42	58.36	45.54	−12.47	−460.35
$(H_3N\cdots NH_3)^+$							
1.00	35.9	7.75	9.01	4.30	−0.59	−6.81	−25.22
1.25	25.9	14.29	15.25	11.49	4.24	−11.57	−78.69
1.50	13.4	20.42	20.98	20.83	13.09	−16.28	−232.54
1.75	4.9	25.81	26.08	30.49	23.95	−19.75	−658.38
$(H_2O\cdots OH_2)^+$							
1.00	39.7	14.19	15.15	7.46	0.17	−11.73	−54.22
1.25	29.1	22.48	23.37	18.43	8.88	−18.80	−178.55
1.50	16.9	29.72	30.27	30.55	21.59	−24.35	−530.66
1.75	9.3	35.32	35.59	41.33	34.38	−27.90	−1462.47
ME		22.21	22.58	21.15	13.39	−10.91	−250.31
MAE		22.21	22.58	21.15	13.46	10.91	250.31
MXE		48.28	48.42	58.36	45.54	27.90	1462.47

[a]The reference is explicitly correlated coupled-cluster theory.[90] For each dimer, calculations were performed at four different intermonomeric distances d_{MM} measured by the ratio d_{MM}/d^0_{MM}, where d^0_{MM} is the equilibrium distance.

are similar. This suggests that the screening in SOSEX is too weak to sufficiently correct bare SOX, which becomes unphysical for higher coupling strengths.

5.5.3. Noncovalent Interaction Energies. The accurate prediction of noncovalent interactions is important for, e.g., diastereoselective reactions.[103] Accuracy within a fraction of a kcal/mol is often desired for these weak interactions, posing a challenging requirement for electronic structure methods. Here we test our implementations on *n*-alkane dimers in the ADIM6 benchmark set.[100] Basis set extrapolations using the Dunning basis sets were performed to investigate basis set convergence because RPA noncovalent interaction energies have been shown to be strongly affected by basis set incompleteness.[104]

As shown in Tables 7 and S3, RPA, AXK, and SOSEX give similar results, with the AXK and SOSEX results being slightly more accurate than those of RPA. For all three methods, the AVTZ basis set overbinds the dimers and yields larger errors for larger systems, while the AVQZ basis set fortuitously gives consistently small errors for all systems (Table S3). In the 3-4 extrapolated CBS limit, the MAEs are below 62, 51, and 51% of the smallest interaction energy within the benchmark set for RPA, AXK, and SOSEX, respectively. Table 7 also lists the results using the QZVPP basis set. Similar to the RPA case,[104] the Karlsruhe quadruple-ζ basis sets provide a good balance between computational cost and accuracy for most practical calculations.

5.5.4. Charged Dimer Dissociation Energies. To assess the magnitude of the self-correlation error in RPA and beyond-RPA methods, dissociation energies of radical cations of symmetric dimers contained in the SIE4x4 benchmark set[90] were computed at various intermonomeric distances; see Table 8. In these radical cations, the positive charge is excessively delocalized in semilocal DFT, producing overbinding and artificial barriers along the potential energy surface.[105] The errors are particularly large for stretched dimers, reflecting incorrect fractional charges[106] in the semilocal DFT picture. RPA removes self-interaction to the first order due to exact first-order exchange, but the missing higher-order terms in the RPA correlation energy still cause a significant self-correlation error. The AXK results are consistently more accurate than the semilocal DFT and RPA ones. In particular, AXK remains fairly accurate close to the equilibrium structures. SOSEX is constructed to be one-electron self-correlation-free. Indeed, SOSEX is nearly exact for H_2^+; the small errors result from the use of TPSS densities to evaluate the energy. The SOSEX dissociation energies are also more accurate at large dimer separations. Nevertheless, SOSEX is less accurate than RPA and AXK for the dissociations of $(NH_3)_2^+$ and $(H_2O)_2^+$ close to the equilibrium intermonomeric distances. This illustrates that freedom from one-electron self-interaction does not necessarily translate to many-electron systems.[107,108]

Radical cations at stretched intermonomeric distances are highly challenging for beyond-RPA perturbative methods, as reflected by the AXK and SOSEX MAEs being greater than 10 kcal/mol for the SIE4x4 benchmark. The catastrophic failure of bare SOX for these systems also suggests that perturbative corrections are inadequate here and points to a need for self-consistent approaches.[109]

5.5.5. Transition-Metal Compound Dissociation Energies. Finally, we assess the implemented methods using a set of 3d transition-metal dissociation reactions proposed in ref 76. This benchmark contains dissociation reactions of 22 transition-metal compounds that represent diverse types of transition-metal bonding. Many species involved in these reactions are small-gap open-shell systems, which provide a demanding test for electronic structure methods. The reference values are

DOI: 10.1021/acs.jctc.8b00777
J. Chem. Theory Comput. 2018, 14, 5701−5714

Table 9. Errors of Calculated Dissociation Energies in kcal/mol of the 3d Transition-Metal Reference Set Relative to Back-Corrected Experimental Values from Reference 76

		TPSS	TPSS-D3	RPA		AXK		SOSEX		SOX
reaction	ref	QZVPP	QZVPP	QZVPP	CBS	QZVPP	CBS	QZVPP	CBS	QZVPP
$Sc_2 \rightarrow 2Sc$	39.8	−7.51	−7.47	−19.70	−20.52	−32.43	−32.57	−48.16	−48.04	−158.78
$V_2 \rightarrow 2V$	64.6	−0.12	−0.12	−15.97	−16.88	−34.60	−28.71	−60.93	−55.50	−293.63
$Ni_2 \rightarrow 2Ni$	49.7	8.31	8.34	−11.80	−11.42	−33.72	−32.15	−84.57	−82.81	−803.58
$CrH \rightarrow Cr + H$	45.7	11.72	11.72	6.75	4.01	6.06	5.46	2.41	2.18	−8.65
$MnH \rightarrow Mn + H$	32.3	20.04	20.07	3.19	3.23	1.77	1.45	2.06	1.76	3.43
$CoH \rightarrow Co + H$	46.6	17.87	17.88	14.41	15.54	16.47	18.52	13.87	13.23	2.91
$TiO \rightarrow Ti + O$	158.8	17.37	17.37	0.40	2.51	−3.28	−0.62	−9.85	−7.01	−49.01
$MnO \rightarrow Mn + O$	91.1	29.21	29.21	−6.01	−3.63	−20.00	−16.73	−35.52	−32.16	−107.22
$CuO \rightarrow Cu + O$	63.7	9.49	9.49	−0.90	−2.09	−5.91	−5.80	−17.75	−17.46	−71.73
$ScF \rightarrow Sc + F$	143.0	8.44	8.44	−6.00	−5.33	−5.65	−4.68	−7.20	−6.09	−20.11
$CrF \rightarrow Cr + F$	105.1	12.82	12.83	1.71	0.56	1.72	2.27	−0.84	0.05	−15.39
$CuF \rightarrow Cu + F$	102.5	−2.91	−2.90	−11.73	−11.36	−10.02	−9.25	−12.23	−11.35	−27.84
$Fe_2Cl_4 \rightarrow 2FeCl_2$	35.0	−8.29	−6.42	−3.79	−1.94	−1.86	0.13	−0.07	1.47	4.09
$CoCl_3 \rightarrow (1/2)Cl_2 + CoCl_2$	16.7	9.48	10.50	1.71	0.67	−9.78	−10.39	−21.24	−21.75	−90.46
$Fe(CO)_5 \rightarrow Fe(CO)_4 + CO$	42.2	4.31	6.00	−3.07	−4.37	−2.73	−3.54	1.50	0.81	15.97
$Ni(CO)_4 \rightarrow Ni(CO)_3 + CO$	24.9	3.95	5.17	−0.36	−4.56	−2.75	−5.64	−2.71	−5.37	−14.08
$(1/2)CrBz_2 \rightarrow (1/2)Cr + Bz$	31.8	6.90	10.06	8.75	0.32	3.13	−0.66	−2.72	−5.70	−37.84
$(1/2)FeCp_2 \rightarrow (1/2)Fe + Cp$	80.1	14.67	18.61	11.88	8.53	8.25	6.82	8.62	7.41	6.65
ME		8.65	9.38	−1.70	−2.60	−6.96	−6.45	−15.30	−14.80	−92.51
MAE		10.75	11.26	7.12	6.53	11.12	10.30	18.46	17.79	96.19
MXE		29.21	29.21	19.70	20.52	34.60	32.57	84.57	48.04	803.58

based on high-quality experimental data and are corrected for zero-point and thermal vibrational energies and scalar-relativistic effects.

All calculations were performed using TPSS structures reported in ref 76, except for Fe_2Cl_4 and $CoCl_3$, for which D_{2h} and D_{3h} structures, respectively, were found to yield lower ground-state energies.[110] As summarized in Tables 9 and S4, the accuracy of each method varies considerably with different types of compounds. The TPSS results confirm that the errors from meta-GGA calculations are around 10 kcal/mol per bond.[76] In general, RPA reduces the errors, but there exist cases where RPA gives less accurate results than TPSS, e.g., metal dimers. The AXK MAE is slightly higher than that of RPA, yet this deterioration is due to only a few types of molecules, as will be discussed below. In general, AXK performs well if the corresponding RPA error is already small. SOSEX and SOX are generally less accurate than AXK.

For RPA and the beyond-RPA methods, the metal dimers give rise to the largest errors in the predicted dissociation energies. These dimers, Sc_2, V_2, and Ni_2, exhibit strong static correlation due to the left−right effect and the near degeneracy of the 4s and 3d subshells.[111] For these systems, semilocal functionals such as TPSS give relatively accurate results in comparison with hybrid functionals[76] and RPA. This trend is related to the XC hole being short-ranged for systems with strong static correlation.[112] The deficiency of RPA in accounting for strong static correlation renders it a poor starting point for perturbative corrections. Consequently, the AXK corrections are in the wrong direction, and both SOSEX and SOX give qualitatively wrong results.

Other types of molecules where the AXK error is significantly larger than that of RPA are the monoxides, particularly MnO. Again, SOSEX and SOX errors are even larger. This trend is consistent with previous calculations on metal monoxides with structures optimized using each respective method. Nevertheless, ref 38 points out that, although AXK worsens RPA for dissociation energies, the former leads to smaller errors in bond lengths and frequencies.

Somewhat surprisingly, for CoH dissociation, bare SOX is more accurate than AXK and SOSEX; a similar trend is observed for the homolytic dissociation of ferrocene, $(1/2)FeCp_2 \rightarrow (1/2)Fe + Cp$. The good accuracy of bare SOX in these cases might result from fortuitous cancellation of higher-order corrections, which is incompletely captured by AXK and SOSEX. To further understand this result, we consider the heterolytic dissociation energy of ferrocene, i.e., $(1/2)FeCp_2 \rightarrow (1/2)Fe^{2+} + Cp^-$, where the experimental value after correcting for scalar-relativistic, zero-point vibrational, and thermal energies is 318 kcal/mol.[113] With the QZVPP basis set, RPA overestimates the homolytic dissociation energy by 6.8 kcal/mol, while AXK and SOSEX underestimate by 4.4 and 13.8 kcal/mol, respectively. Unlike homolytic ferrocene dissociation, the heterolytic dissociation energy is severely underestimated by bare SOX, which yields an error of −64.2 kcal/mol. The magnitude of the SOX error is comparable to that of the MP2 CBS calculation in the literature, which is 59 kcal/mol too high.[114] The large negative SOX error suggests that ferrocene is relatively strongly correlated and thus confirms the error cancellation in the SOX calculation for the homolytic ferrocene dissociation.

6. DISCUSSION

The above results suggest a simple explanation for when and why perturbative corrections to RPA break down. At higher coupling strength, any low-order corrections and RPA itself eventually become unphysical. A qualitative measure of correlation strength is the relative difference between the AXK and SOX beyond-RPA correlation energies

$$\bar{\alpha} = \frac{\Delta E^{\mathrm{C\,SOX}} - \Delta E^{\mathrm{C\,AXK}}}{\Delta E^{\mathrm{C\,SOX}}} \tag{28}$$

DOI: 10.1021/acs.jctc.8b00777
J. Chem. Theory Comput. 2018, 14, 5701−5714

$\bar{\alpha}$ is non-negative and goes to zero as AXK approaches SOX for small coupling. With increasing coupling strength, AXK but not SOX is screened, giving rise to more positive $\bar{\alpha}$ values. $\bar{\alpha}$ may be understood as an effective average coupling strength for beyond-RPA correlation. This concept may be extended to energy differences by defining $\bar{\alpha}$ as the maximum of the individual $\bar{\alpha}$ values of all involved species.

Figure 4 shows that $\bar{\alpha}$ is positively correlated with the absolute error of AXK. When $\bar{\alpha}$ is greater than 0.5, the SOX

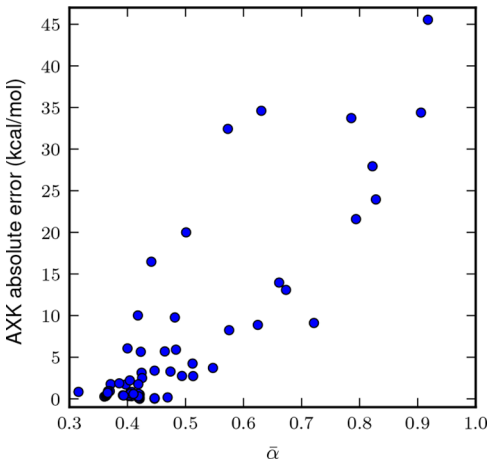

Figure 4. Correlation between the absolute error of AXK and the $\bar{\alpha}$ value for all of the QZVPP energy difference calculations for the BHDIV10, DARC, ADIM6, and SIE4x4 benchmark sets[90] as well as the 3d transition-metal reference set.[76]

beyond-RPA correlation energy is more than twice that of AXK. For such systems, AXK typically does not deliver acceptable accuracy. This suggests that $\bar{\alpha}$ may be used as a diagnostic for the reliability of AXK.

Large $\bar{\alpha}$ values, however, do not always imply incorrect results. For the first CO dissociation of $Fe(CO)_5$ and the homolytic dissociation of ferrocene, the $\bar{\alpha}$ values are 0.51 and 0.58, but the AXK errors are −2.71 and 8.62 kcal/mol, respectively. This unexpectedly good accuracy of AXK for these two reactions may be attributed to error cancellation between the reactants and the products.

Ni_2 exhibits an $\bar{\alpha}$ value of 0.79, the largest among all species in the 3d transition-metal reference set. (Even higher $\bar{\alpha}$ values are observed for charged dimers in the SIE4x4 benchmark set but not at equilibrium distances.) The coupling strength integrands ΔU_α^C of the beyond-RPA correlation energy of Ni_2 for SOX, SOSEX, and AXK are plotted in Figure 5; the total beyond-RPA correlation energy is the coupling strength average[47,115]

$$\Delta E^C = \int_0^1 d\alpha\, \Delta U_\alpha^C \tag{29}$$

Although the $\Delta U_\alpha^{C\ AXK}$ curve tends to the linear SOX integrand at $\alpha = 0$, it is rapidly screened at larger coupling strength, which is reflected in the high value of $\bar{\alpha}$. Figure 5 also reveals a simple geometrical meaning of $\bar{\alpha}$: it measures the relative difference of the area under the SOX and AXK coupling strength integrands. For Ni_2, even the strong AXK screening is insufficient, as reflected in the large AXK error of the Ni_2 binding energy.

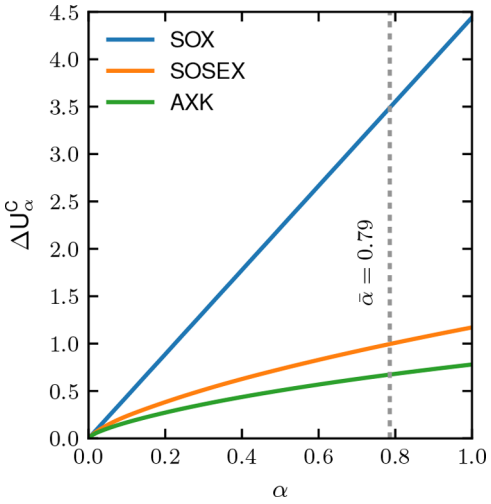

Figure 5. Coupling strength dependence of $\Delta U_\alpha^{C\ AXK}$, $\Delta U_\alpha^{C\ SOSEX}$, and $\Delta U_\alpha^{C\ SOX}$ for Ni_2. The area under each curve is the beyond-RPA correlation energy of the corresponding method. The AXK and SOSEX calculations were performed with a seven-point Gauss−Legendre coupling strength quadrature using the QZVPP basis set. The effective coupling strength $\bar{\alpha}$ equals the relative difference of the areas under the SOX and AXK curves.

7. CONCLUSIONS

Two efficient and robust implementations of the AXK methods using the RI approximation and numerical frequency integration were presented: The AO based $O(N^4 \ln N)$ algorithm is fast for molecules of over 200 atoms with small basis sets, while the MO based $O(N^5 \ln N)$ algorithm enables calculations on a single workstation computer for molecules of up to 100 atoms with triple- and quadruple-ζ basis sets, which are necessary for accurate energy difference predictions. The bare SOX and SOSEX beyond-RPA correlation energies can also be computed using these algorithms, facilitating comparison of these methods for large systems.

The AXK method yields improved accuracy for ground-state energy differences of systems with relatively weak correlation. Systematic improvement over RPA is observed for reaction barrier heights, reaction energies, and noncovalent interaction energies of main-group compounds. In these benchmarks, AXK reduces RPA errors by 25−50% and outperforms SOSEX. In particular, for the DARC benchmark, the AXK errors are less than half of the RPA errors on average and are an order of magnitude lower than those of SOSEX. These systems are characterized by relatively small average coupling strengths $\bar{\alpha}$, and thus, perturbative corrections are viable. For these weakly correlated systems, including higher-order terms in the geometric series expansion of eq 15, along the lines recently proposed by Bates and co-workers,[115] is likely to yield further accuracy gains. The increased computational effort of AXK compared with bare RPA may be particularly worthwhile for systems with small but non-negligible $\bar{\alpha}$ values, where bare perturbation theory such as MP2 is insufficient and coupled-cluster methods are too costly.

For systems with strong correlation, indicated by effective coupling strength values of 0.5 or above, perturbative beyond-RPA corrections break down because the underlying assumption that "XC kernel corrections" are small is no longer justified. Indeed, RPA itself relies on this assumption and becomes an increasingly unphysical reference with increasing

DOI: 10.1021/acs.jctc.8b00777
J. Chem. Theory Comput. 2018, 14, 5701−5714

coupling strength. Such strongly correlated systems include transition-metal compounds exhibiting strong static correlations or metallic systems at low electron density.

An additional source of errors independent of the effective coupling strength is inaccuracies in the KS input orbitals, or "density-driven errors".[116] These types of errors are addressed by variational self-consistent approaches such as generalized KS RPA.[109]

APPENDIX: VARIATIONAL BOUNDEDNESS OF RI-RPA CORRELATION ENERGY

Reference 41 showed that the RI-RPA correlation energy $\tilde{E}^{\mathrm{C\ RPA}}$ is an upper bound of the exact RPA correlation energy $E^{\mathrm{C\ RPA}}$. However, the proof therein assumes that the RI error in the direct ring coupled-cluster doubles amplitude is negligible. This Appendix presents a more general proof without this assumption. Throughout this Appendix, tildes denote quantities with the RI approximation, while quantities without tildes are associated with the full-rank representation.

The RI counterpart of eq 6 can be written as

$$\tilde{\mathbf{B}}^{\mathrm{H}} = \tilde{\mathbf{S}}\tilde{\mathbf{S}}^{\mathrm{T}} \tag{30}$$

where

$$\tilde{S}_{iaP} = (ia|\bar{P}) \tag{31}$$

is an $N_{\mathrm{h}}N_{\mathrm{p}} \times N_{\mathrm{aux}}$ matrix as defined in section 3.1; the bar notation denotes orthonormalized vectors in the space with an inner product defined by the Coulomb integrals, i.e.

$$|\bar{P}) = \sum_{Q} |Q)[\mathbf{L}^{-1}]_{QP} \tag{32}$$

$\tilde{\mathbf{S}}$ is related to the full-rank $\mathbf{S}$ defined in eq 6 through a matrix $\mathbf{U}$

$$\tilde{\mathbf{S}} = \mathbf{S}\mathbf{U} \tag{33}$$

It is readily shown that

$$\mathbf{U}^{\mathrm{T}}\mathbf{U} = \tilde{\mathbf{S}}^{\mathrm{T}}(\mathbf{B}^{\mathrm{H}})^{-1}\tilde{\mathbf{S}} \tag{34}$$

and

$$[\mathbf{U}^{\mathrm{T}}\mathbf{U}]_{PQ} = \sum_{ia} (\bar{P}|\overline{ia})(\overline{ia}|\bar{Q}) \tag{35}$$

where

$$|\overline{ia}) = \sum_{jb} |jb)[\mathbf{S}^{-1}]_{jbia} \tag{36}$$

Lemma A.1. For any N_{aux}-dimensional unit vector $\mathbf{v}$

$$\mathbf{v}^{\mathrm{T}}\mathbf{U}^{\mathrm{T}}\mathbf{U}\mathbf{v} \le 1 \tag{37}$$

Proof: Define $|v) = \sum_P |\bar{P})v_P$. This is a unit vector in the inner product space. The conclusion follows from eq 35.

Theorem A.2. Let $q_1(\omega) \le \cdots \le q_{N_{\mathrm{h}}N_{\mathrm{p}}}(\omega)$ and $\tilde{q}_1(\omega) \le \cdots \le \tilde{q}_{N_{\mathrm{aux}}}(\omega)$ be the eigenvalues of $\mathbf{Q}(\omega)$ and $\tilde{\mathbf{Q}}(\omega)$, respectively. They satisfy

$$0 \le \tilde{q}_P(\omega) \le q_{N_{\mathrm{h}}N_{\mathrm{p}}-N_{\mathrm{aux}}+P}(\omega) \tag{38}$$

for $1 \le P \le N_{\mathrm{aux}}$.

Proof: By definition, eq 13, $\tilde{\mathbf{Q}}(\omega)$ is related to $\mathbf{Q}(\omega)$ through

$$\tilde{\mathbf{Q}}(\omega) = \mathbf{U}^{\mathrm{T}}\mathbf{Q}(\omega)\mathbf{U} \tag{39}$$

The rest of the proof closely follows the proof of the Cauchy interlacing property from the Courant–Fischer min–max theorem. The only difference is that $\mathbf{U}^{\mathrm{T}}\mathbf{U}$ is not an orthogonal projection here but satisfies eq 37. As a result, only "half" of the interlacing property can be shown, as stated in this theorem.

Theorem A.3. $E^{\mathrm{C\ RPA}} \le \tilde{E}^{\mathrm{C\ RPA}}$.

Proof: The RPA correlation energy, eq 12, may be rewritten as

$$E^{\mathrm{C\ RPA}} = \frac{1}{2\pi}\int_0^\infty \mathrm{d}\omega \sum_{P=1}^{N_{\mathrm{h}}N_{\mathrm{p}}} g(q_P(\omega)) \tag{40}$$

where g is defined on $[0, \infty)$ by $g(x) = -x^2 f_1(x) = \ln(1 + x) - x$. Because g is nonpositive and monotonically decreasing, we see that

$$E^{\mathrm{C\ RPA}} \le \frac{1}{2\pi}\int_0^\infty \mathrm{d}\omega \sum_{P=1}^{N_{\mathrm{aux}}} g(q_{N_{\mathrm{h}}N_{\mathrm{p}}-N_{\mathrm{aux}}+P}(\omega)) \tag{41}$$

$$\le \frac{1}{2\pi}\int_0^\infty \mathrm{d}\omega \sum_{P=1}^{N_{\mathrm{aux}}} g(\tilde{q}_P(\omega)) \tag{42}$$

$$= \tilde{E}^{\mathrm{C\ RPA}} \tag{43}$$

ASSOCIATED CONTENT

Supporting Information

The Supporting Information is available free of charge on the ACS Publications website at DOI: 10.1021/acs.jctc.8b00777.

Pseudocodes of the RI-AXK algorithms and benchmark results using various basis sets (PDF)

AUTHOR INFORMATION

Corresponding Author

*E-mail: filipp.furche@uci.edu.

ORCID

Guo P. Chen: 0000-0002-4743-4450

Filipp Furche: 0000-0001-8520-3971

Funding

This material is based upon work supported by the National Science Foundation under CHE-1464828 and CHE-1800431.

Notes

The authors declare the following competing financial interest(s): Principal investigator Filipp Furche has an equity interest in Turbomole GmbH. The terms of this arrangement have been reviewed and approved by the University of California, Irvine, in accordance with its conflict of interest policies.

ACKNOWLEDGMENTS

G.P.C. thanks Dr. Shane M. Parker for providing optimized structures of mesityl-substituted porphyrins and is grateful to Dr. Vamsee K. Voora and Sree Ganesh Balasubramani for helpful discussions.

REFERENCES

(1) Heßelmann, A.; Görling, A. Random-Phase Approximation Correlation Methods for Molecules and Solids. *Mol. Phys.* **2011**, *109*, 2473–2500.

(2) Eshuis, H.; Bates, J. E.; Furche, F. Electron Correlation Methods Based on the Random Phase Approximation. *Theor. Chem. Acc.* **2012**, *131*, 1084.

DOI: 10.1021/acs.jctc.8b00777
J. Chem. Theory Comput. 2018, 14, 5701–5714

(3) Ren, X.; Rinke, P.; Joas, C.; Scheffler, M. Random-Phase Approximation and Its Applications in Computational Chemistry and Materials Science. *J. Mater. Sci.* **2012**, *47*, 7447−7471.
(4) Chen, G. P.; Voora, V. K.; Agee, M. M.; Balasubramani, S. G.; Furche, F. Random-Phase Approximation Methods. *Annu. Rev. Phys. Chem.* **2017**, *68*, 421−445.
(5) Møller, C.; Plesset, M. S. Note on an Approximation Treatment for Many-Electron Systems. *Phys. Rev.* **1934**, *46*, 618−622.
(6) Harl, J.; Kresse, G. Accurate Bulk Properties from Approximate Many-Body Techniques. *Phys. Rev. Lett.* **2009**, *103*, 056401.
(7) Dobson, J. F.; Wang, J. Successful Test of a Seamless van der Waals Density Functional. *Phys. Rev. Lett.* **1999**, *82*, 2123−2126.
(8) Lebègue, S.; Harl, J.; Gould, T.; Ángyán, J. G.; Kresse, G.; Dobson, J. F. Cohesive Properties and Asymptotics of the Dispersion Interaction in Graphite by the Random Phase Approximation. *Phys. Rev. Lett.* **2010**, *105*, 196401.
(9) Eshuis, H.; Furche, F. A Parameter-Free Density Functional That Works for Noncovalent Interactions. *J. Phys. Chem. Lett.* **2011**, *2*, 983−989.
(10) Furche, F. Molecular Tests of the Random Phase Approximation to the Exchange-Correlation Energy Functional. *Phys. Rev. B: Condens. Matter Mater. Phys.* **2001**, *64*, 195120.
(11) Fuchs, M.; Niquet, Y.-M.; Gonze, X.; Burke, K. Describing Static Correlation in Bond Dissociation by Kohn-Sham Density Functional Theory. *J. Chem. Phys.* **2005**, *122*, 094116.
(12) Singwi, K. S.; Tosi, M. P.; Land, R. H.; Sjölander, A. Electron Correlations at Metallic Densities. *Phys. Rev.* **1968**, *176*, 589−599.
(13) Freeman, D. L. Coupled-Cluster Expansion Applied to the Electron Gas: Inclusion of Ring and Exchange Effects. *Phys. Rev. B* **1977**, *15*, 5512−5521.
(14) Kurth, S.; Perdew, J. Density-Functional Correction of Random-Phase-Approximation Correlation with Results for Jellium Surface Energies. *Phys. Rev. B: Condens. Matter Mater. Phys.* **1999**, *59*, 10461−10468.
(15) Yan, Z.; Perdew, J.; Kurth, S. Density Functional for Short-Range Correlation: Accuracy of the Random-Phase Approximation for Isoelectronic Energy Changes. *Phys. Rev. B: Condens. Matter Mater. Phys.* **2000**, *61*, 16430−16439.
(16) Janesko, B. G.; Henderson, T. M.; Scuseria, G. E. Long-Range-Corrected Hybrids Including Random Phase Approximation Correlation. *J. Chem. Phys.* **2009**, *130*, 081105.
(17) Janesko, B. G.; Henderson, T. M.; Scuseria, G. E. Long-Range-Corrected Hybrid Density Functionals Including Random Phase Approximation Correlation: Application to Noncovalent Interactions. *J. Chem. Phys.* **2009**, *131*, 034110.
(18) Toulouse, J.; Gerber, I. C.; Jansen, G.; Savin, A.; Ángyán, J. G. Adiabatic-Connection Fluctuation-Dissipation Density-Functional Theory Based on Range Separation. *Phys. Rev. Lett.* **2009**, *102*, 096404.
(19) Toulouse, J.; Zhu, W.; Ángyán, J. G.; Savin, A. Range-Separated Density-Functional Theory with the Random-Phase Approximation: Detailed Formalism and Illustrative Applications. *Phys. Rev. A: At., Mol., Opt. Phys.* **2010**, *82*, 032502.
(20) Ruzsinszky, A.; Perdew, J. P.; Csonka, G. I. The RPA Atomization Energy Puzzle. *J. Chem. Theory Comput.* **2010**, *6*, 127−134.
(21) Ruzsinszky, A.; Perdew, J. P.; Csonka, G. I. A Simple but Fully Nonlocal Correction to the Random Phase Approximation. *J. Chem. Phys.* **2011**, *134*, 114110.
(22) Dobson, J. F.; Wang, J.; Gould, T. Correlation Energies of Inhomogeneous Many-Electron Systems. *Phys. Rev. B: Condens. Matter Mater. Phys.* **2002**, *66*, 081108.
(23) Furche, F.; Van Voorhis, T. Fluctuation-Dissipation Theorem Density-Functional Theory. *J. Chem. Phys.* **2005**, *122*, 164106.
(24) Dobson, J. F.; Wang, J. Energy-Optimized Local Exchange-Correlation Kernel for the Electron Gas: Application to van der Waals Forces. *Phys. Rev. B: Condens. Matter Mater. Phys.* **2000**, *62*, 10038−10045.
(25) Bates, J. E.; Laricchia, S.; Ruzsinszky, A. Nonlocal Energy-Optimized Kernel: Recovering Second-Order Exchange in the Homogeneous Electron Gas. *Phys. Rev. B: Condens. Matter Mater. Phys.* **2016**, *93*, 045119.
(26) Ruzsinszky, A.; Constantin, L. A.; Pitarke, J. M. Kernel-Corrected Random-Phase Approximation for the Uniform Electron Gas and Jellium Surface Energy. *Phys. Rev. B: Condens. Matter Mater. Phys.* **2016**, *94*, 165155.
(27) Olsen, T.; Thygesen, K. S. Extending the Random-Phase Approximation for Electronic Correlation Energies: The Renormalized Adiabatic Local Density Approximation. *Phys. Rev. B: Condens. Matter Mater. Phys.* **2012**, *86*, 081103.
(28) Olsen, T.; Thygesen, K. S. Accurate Ground-State Energies of Solids and Molecules from Time-Dependent Density-Functional Theory. *Phys. Rev. Lett.* **2014**, *112*, 203001.
(29) Constantin, L. A.; Pitarke, J. M. Simple Dynamic Exchange-Correlation Kernel of a Uniform Electron Gas. *Phys. Rev. B: Condens. Matter Mater. Phys.* **2007**, *75*, 245127.
(30) Trevisanutto, P. E.; Terentjevs, A.; Constantin, L. A.; Olevano, V.; Sala, F. D. Optical Spectra of Solids Obtained by Time-Dependent Density Functional Theory with the Jellium-With-Gap-Model Exchange-Correlation Kernel. *Phys. Rev. B: Condens. Matter Mater. Phys.* **2013**, *87*, 205143.
(31) Gell-Mann, M.; Brueckner, K. A. Correlation Energy of an Electron Gas at High Density. *Phys. Rev.* **1957**, *106*, 364−368.
(32) Pines, D. A Collective Description of Electron Interactions: IV. Electron Interaction in Metals. *Phys. Rev.* **1953**, *92*, 626−636.
(33) Grüneis, A.; Marsman, M.; Harl, J.; Schimka, L.; Kresse, G. Making the Random Phase Approximation to Electronic Correlation Accurate. *J. Chem. Phys.* **2009**, *131*, 154115.
(34) Ángyán, J. G.; Liu, R.-F.; Toulouse, J.; Jansen, G. Correlation Energy Expressions from the Adiabatic-Connection Fluctuation−Dissipation Theorem Approach. *J. Chem. Theory Comput.* **2011**, *7*, 3116−3130.
(35) Henderson, T. M.; Scuseria, G. E. The Connection Between Self-Interaction and Static Correlation: A Random Phase Approximation Perspective. *Mol. Phys.* **2010**, *108*, 2511−2517.
(36) Paier, J.; Ren, X.; Rinke, P.; Scuseria, G. E.; Grüneis, A.; Kresse, G.; Scheffler, M. Assessment of Correlation Energies Based on the Random-Phase Approximation. *New J. Phys.* **2012**, *14*, 043002.
(37) Ren, X.; Rinke, P.; Scuseria, G. E.; Scheffler, M. Renormalized Second-Order Perturbation Theory for the Electron Correlation Energy: Concept, Implementation, and Benchmarks. *Phys. Rev. B: Condens. Matter Mater. Phys.* **2013**, *88*, 035120.
(38) Bates, J. E.; Furche, F. Communication: Random Phase Approximation Renormalized Many-Body Perturbation Theory. *J. Chem. Phys.* **2013**, *139*, 171103.
(39) Salpeter, E. E.; Bethe, H. A. A Relativistic Equation for Bound-State Problems. *Phys. Rev.* **1951**, *84*, 1232−1242.
(40) Onida, G.; Reining, L.; Rubio, A. Electronic Excitations: Density-Functional versus Many-Body Green's-Function Approaches. *Rev. Mod. Phys.* **2002**, *74*, 601−659.
(41) Eshuis, H.; Yarkony, J.; Furche, F. Fast Computation of Molecular Random Phase Approximation Correlation Energies Using Resolution of the Identity and Imaginary Frequency Integration. *J. Chem. Phys.* **2010**, *132*, 234114.
(42) Ren, X.; Rinke, P.; Scuseria, G. E.; Scheffler, M. Renormalized Second-Order Perturbation Theory for the Electron Correlation Energy: Concept, Implementation, and Benchmarks. *Phys. Rev. B: Condens. Matter Mater. Phys.* **2013**, *88*, 035120.
(43) Mussard, B.; Rocca, D.; Jansen, G.; Ángyán, J. G. Dielectric Matrix Formulation of Correlation Energies in the Random Phase Approximation: Inclusion of Exchange Effects. *J. Chem. Theory Comput.* **2016**, *12*, 2191−2202.
(44) Dixit, A.; Ángyán, J. G.; Rocca, D. Improving the Accuracy of Ground-State Correlation Energies within a Plane-Wave Basis Set: The Electron-Hole Exchange Kernel. *J. Chem. Phys.* **2016**, *145*, 104105.

DOI: 10.1021/acs.jctc.8b00777
J. Chem. Theory Comput. 2018, 14, 5701−5714

(45) Dixit, A.; Claudot, J.; Lebègue, S.; Rocca, D. Improving the Efficiency of Beyond-RPA Methods within the Dielectric Matrix Formulation: Algorithms and Applications to the A24 and S22 Test Sets. *J. Chem. Theory Comput.* **2017**, *13*, 5432−5442.
(46) Beuerle, M.; Graf, D.; Schurkus, H. F.; Ochsenfeld, C. Efficient Calculation of Beyond RPA Correlation Energies in the Dielectric Matrix Formalism. *J. Chem. Phys.* **2018**, *148*, 204104.
(47) Langreth, D. C.; Perdew, J. P. The Exchange-Correlation Energy of a Metallic Surface. *Solid State Commun.* **1975**, *17*, 1425−1429.
(48) Langreth, D.; Perdew, J. Exchange-Correlation Energy of a Metallic Surface: Wave-Vector Analysis. *Phys. Rev. B* **1977**, *15*, 2884−2901.
(49) Fetter, A. L.; Walecka, J. D. *Quantum Theory of Many-Particle Systems*; McGrawHill: New York, 1971.
(50) Gunnarsson, O.; Lundqvist, B. I. Exchange and Correlation in Atoms, Molecules, and Solids by Spin-Density Functional Formalism. *Phys. Rev. B* **1976**, *13*, 4274−4298.
(51) Woodbury, M. A. *Inverting Modified Matrices*; Memo. Rep. No. 42; Statistical Research Group, Princeton University: Princeton, NJ, 1950.
(52) Baldereschi, A.; Tosatti, E. Mean-Value Point and Dielectric Properties of Semiconductors and Insulators. *Phys. Rev. B: Condens. Matter Mater. Phys.* **1978**, *17*, 4710−4717.
(53) Govoni, M.; Galli, G. Large Scale GW Calculations. *J. Chem. Theory Comput.* **2015**, *11*, 2680−2696.
(54) Hellgren, M.; von Barth, U. Correlation Energy Functional and Potential from Time-Dependent Exact-Exchange Theory. *J. Chem. Phys.* **2010**, *132*, 044101.
(55) Heßelmann, A.; Görling, A. Random Phase Approximation Correlation Energies with Exact Kohn−Sham Exchange. *Mol. Phys.* **2010**, *108*, 359−372.
(56) McLachlan, A.; Ball, M. Time-Dependent Hartree-Fock Theory for Molecules. *Rev. Mod. Phys.* **1964**, *36*, 844−855.
(57) Klopper, W.; Teale, A. M.; Coriani, S.; Pedersen, T. B.; Helgaker, T. Spin Flipping in Ring-Coupled-Cluster-Doubles Theory. *Chem. Phys. Lett.* **2011**, *510*, 147−153.
(58) von Barth, U.; Hedin, L. A Local Exchange-Correlation Potential for the Spin Polarized Case: I. *J. Phys. C: Solid State Phys.* **1972**, *5*, 1629−1642.
(59) Wang, Y.; Perdew, J. P. Correlation Hole of the Spin-Polarized Electron Gas, with Exact Small-Wave-Vector and High-Density Scaling. *Phys. Rev. B: Condens. Matter Mater. Phys.* **1991**, *44*, 13298−13307.
(60) Gori-Giorgi, P.; Perdew, J. P. Pair Distribution Function of the Spin-Polarized Electron Gas: A First-Principles Analytic Model for All Uniform Densities. *Phys. Rev. B: Condens. Matter Mater. Phys.* **2002**, *66*, 165118.
(61) Whitten, J. L. Coulombic Potential Energy Integrals and Approximations. *J. Chem. Phys.* **1973**, *58*, 4496−4501.
(62) Dunlap, B. I.; Connolly, J. W. D.; Sabin, J. R. On Some Approximations in Applications of Xα Theory. *J. Chem. Phys.* **1979**, *71*, 3396−3402.
(63) Baerends, E. J.; Ellis, D. E.; Ros, P. Self-Consistent Molecular Hartree-Fock-Slater Calculations I. The Computational Procedure. *Chem. Phys.* **1973**, *2*, 41−51.
(64) Vahtras, O.; Almlöf, J.; Feyereisen, M. W. Integral Approximations for LCAO-SCF Calculations. *Chem. Phys. Lett.* **1993**, *213*, 514−518.
(65) Jung, Y.; Sodt, A.; Gill, P. M. W.; Head-Gordon, M. Auxiliary Basis Expansions for Large-Scale Electronic Structure Calculations. *Proc. Natl. Acad. Sci. U. S. A.* **2005**, *102*, 6692−6697.
(66) Reine, S.; Tellgren, E.; Krapp, A.; Kjaergaard, T.; Helgaker, T.; Jansik, B.; Host, S.; Salek, P. Variational and Robust Density Fitting of Four-Center Two-Electron Integrals in Local Metrics. *J. Chem. Phys.* **2008**, *129*, 104101.
(67) Tew, D. P. Communication: Quasi-Robust Local Density Fitting. *J. Chem. Phys.* **2018**, *148*, 011102.
(68) Boyd, J. P. Exponentially Convergent Fourier-Chebshev Quadrature Schemes on Bounded and Infinite Intervals. *J. Sci. Comput.* **1987**, *2*, 99−109.
(69) Lawson, C. L.; Hanson, R. J.; Kincaid, D. R.; Krogh, F. T. Basic Linear Algebra Subprograms for Fortran Usage. *ACM Trans. Math. Softw.* **1979**, *5*, 308−323.
(70) Almlöf, J.; Faegri, K.; Korsell, K. Principles for a Direct SCF Approach to LCAO-MO Ab-Initio Calculations. *J. Comput. Chem.* **1982**, *3*, 385−399.
(71) Häser, M.; Ahlrichs, R. Improvements on the Direct SCF Method. *J. Comput. Chem.* **1989**, *10*, 104−111.
(72) Dagum, L.; Menon, R. OpenMP: An Industry Standard API for Shared-Memory Programming. *IEEE Comput. Sci. Eng.* **1998**, *5*, 46−55.
(73) Furche, F.; Ahlrichs, R.; Hättig, C.; Klopper, W.; Sierka, M.; Weigend, F. Turbomole. *WIREs Comput. Mol. Sci.* **2014**, *4*, 91−100.
(74) Tao, J.; Perdew, J.; Staroverov, V.; Scuseria, G. Climbing the Density Functional Ladder: Nonempirical Meta-Generalized Gradient Approximation Designed for Molecules and Solids. *Phys. Rev. Lett.* **2003**, *91*, 146401.
(75) Staroverov, V. N.; Scuseria, G. E.; Tao, J.; Perdew, J. P. Comparative Assessment of a New Nonempirical Density Functional: Molecules and Hydrogen-Bonded Complexes. *J. Chem. Phys.* **2003**, *119*, 12129.
(76) Furche, F.; Perdew, J. P. The Performance of Semilocal and Hybrid Density Functionals in 3d Transition-Metal Chemistry. *J. Chem. Phys.* **2006**, *124*, 044103.
(77) Treutler, O.; Ahlrichs, R. Efficient Molecular Numerical Integration Schemes. *J. Chem. Phys.* **1995**, *102*, 346.
(78) Weigend, F.; Furche, F.; Ahlrichs, R. Gaussian Basis Sets of Quadruple zeta Valence Quality for Atoms H-Kr. *J. Chem. Phys.* **2003**, *119*, 12753.
(79) Weigend, F.; Ahlrichs, R. Balanced Basis Sets of Split Valence, Triple zeta Valence and Quadruple zeta Valence Quality for H to Rn: Design and Assessment of Accuracy. *Phys. Chem. Chem. Phys.* **2005**, *7*, 3297−3305.
(80) Weigend, F.; Häser, M.; Patzelt, H.; Ahlrichs, R. RI-Mp2: Optimized Auxiliary Basis Sets and Demonstration of Efficiency. *Chem. Phys. Lett.* **1998**, *294*, 143−152.
(81) Hättig, C. Optimization of Auxiliary Basis Sets for RI-MP2 and RI-CC2 Calculations: Core−Valence and Quintuple-ζ Basis Sets for H to Ar and QZVPP Basis Sets for Li to Kr. *Phys. Chem. Chem. Phys.* **2005**, *7*, 59−66.
(82) Helgaker, T.; Klopper, W.; Koch, H.; Noga, J. Basis-Set Convergence of Correlated Calculations on Water. *J. Chem. Phys.* **1997**, *106*, 9639.
(83) Halkier, A.; Helgaker, T.; Jørgensen, P.; Klopper, W.; Koch, H.; Olsen, J.; Wilson, A. K. Basis-Set Convergence in Correlated Calculations on Ne, N_2, and H_2O. *Chem. Phys. Lett.* **1998**, *286*, 243−252.
(84) Dunning, T. H. Gaussian Basis Sets for Use in Correlated Molecular Calculations. I. The Atoms Boron Through Neon and Hydrogen. *J. Chem. Phys.* **1989**, *90*, 1007.
(85) Woon, D. E.; Dunning, T. H. Gaussian Basis Sets for Use in Correlated Molecular Calculations. III. The Atoms Aluminum Through Argon. *J. Chem. Phys.* **1993**, *98*, 1358.
(86) Balabanov, N. B.; Peterson, K. A. Systematically Convergent Basis Sets for Transition Metals. I. All-Electron Correlation Consistent Basis Sets for the 3d Elements Sc-Zn. *J. Chem. Phys.* **2005**, *123*, 064107.
(87) Weigend, F.; Köhn, A.; Hättig, C. Efficient Use of the Correlation Consistent Basis Sets in Resolution of the Identity MP2 Calculations. *J. Chem. Phys.* **2002**, *116*, 3175−3183.
(88) Bross, D. H.; Hill, J. G.; Werner, H.-J.; Peterson, K. A. Explicitly Correlated Composite Thermochemistry of Transition Metal Species. *J. Chem. Phys.* **2013**, *139*, 094302.
(89) Ito, S.; Hiroto, S.; Lee, S.; Son, M.; Hisaki, I.; Yoshida, T.; Kim, D.; Kobayashi, N.; Shinokubo, H. Synthesis of Highly Twisted and

DOI: 10.1021/acs.jctc.8b00777
J. Chem. Theory Comput. 2018, 14, 5701−5714

Fully π-Conjugated Porphyrinic Oligomers. *J. Am. Chem. Soc.* **2015**, *137*, 142−145.
(90) Goerigk, L.; Hansen, A.; Bauer, C.; Ehrlich, S.; Najibi, A.; Grimme, S. A Look at the Density Functional Theory Zoo with the Advanced GMTKN55 Database for General Main Group Thermochemistry, Kinetics and Noncovalent Interactions. *Phys. Chem. Chem. Phys.* **2017**, *19*, 32184−32215.
(91) *GMTKN55 database*. http://www.thch.uni-bonn.de/GMTKN55 (accessed Sept 2, 2018).
(92) Latała, R. Some Estimates of Norms of Random Matrices. *Proc. Am. Math. Soc.* **2005**, *133*, 1273−1282.
(93) Johnson, E. R.; Mori-Sánchez, P.; Cohen, A. J.; Yang, W. Delocalization Errors in Density Functionals and Implications for Main-Group Thermochemistry. *J. Chem. Phys.* **2008**, *129*, 204112.
(94) Goerigk, L.; Grimme, S. A General Database for Main Group Thermochemistry, Kinetics, and Noncovalent Interactions − Assessment of Common and Reparameterized (meta-)GGA Density Functionals. *J. Chem. Theory Comput.* **2010**, *6*, 107−126.
(95) Nakano, H.; Nakayama, K.; Hirao, K.; Dupuis, M. Transition State Barrier Height for the Reaction $H_2CO \rightarrow H_2 + CO$ Studied by Multireference Møller−Plesset Perturbation Theory. *J. Chem. Phys.* **1997**, *106*, 4912−4917.
(96) Zhang, Y.; Yang, W. A Challenge for Density Functionals: Self-Interaction Error Increases for Systems with a Noninteger Number of Electrons. *J. Chem. Phys.* **1998**, *109*, 2604−2608.
(97) Cohen, A. J.; Mori-Sánchez, P.; Yang, W. Challenges for Density Functional Theory. *Chem. Rev.* **2012**, *112*, 289−320.
(98) Zhao, Y.; Gonzalez-Garcia, N.; Truhlar, D. G. Benchmark Database of Barrier Heights for Heavy Atom Transfer, Nucleophilic Substitution, Association, and Unimolecular Reactions and Its Use to Test Theoretical Methods. *J. Phys. Chem. A* **2005**, *109*, 2012−2018.
(99) Zheng, J.; Zhao, Y.; Truhlar, D. G. The DBH24/08 Database and Its Use to Assess Electronic Structure Model Chemistries for Chemical Reaction Barrier Heights. *J. Chem. Theory Comput.* **2009**, *5*, 808−821.
(100) Grimme, S.; Antony, J.; Ehrlich, S.; Krieg, H. A Consistent and Accurate Ab Initio Parametrization of Density Functional Dispersion Correction (DFT-D) for the 94 Elements H-Pu. *J. Chem. Phys.* **2010**, *132*, 154104.
(101) Ruzsinszky, A.; Zhang, I. Y.; Scheffler, M. Insight into Organic Reactions from the Direct Random Phase Approximation and Its Corrections. *J. Chem. Phys.* **2015**, *143*, 144115.
(102) Hartley, M. K.; Vine, S.; Walsh, E.; Avrantinis, S.; Daub, G. W.; Cave, R. J. Comparison of Relative Activation Energies Obtained by Density Functional Theory and the Random Phase Approximation for Several Claisen Rearrangements. *J. Phys. Chem. B* **2016**, *120*, 1486−1496.
(103) Tao, D. J.; Muuronen, M.; Slutskyy, Y.; Le, A.; Furche, F.; Overman, L. E. Diastereoselective Coupling of Chiral Acetonide Trisubstituted Radicals with Alkenes. *Chem. Eur. J.* **2016**, *22*, 8786−8790.
(104) Eshuis, H.; Furche, F. Basis Set Convergence of Molecular Correlation Energy Differences within the Random Phase Approximation. *J. Chem. Phys.* **2012**, *136*, 084105.
(105) Braïda, B.; Hiberty, P. C.; Savin, A. A Systematic Failing of Current Density Functionals: Overestimation of Two-Center Three-Electron Bonding Energies. *J. Phys. Chem. A* **1998**, *102*, 7872−7877.
(106) Cohen, A. J.; Mori-Sánchez, P.; Yang, W. Insights into Current Limitations of Density Functional Theory. *Science* **2008**, *321*, 792−794.
(107) Mori-Sánchez, P.; Cohen, A. J.; Yang, W. Many-Electron Self-Interaction Error in Approximate Density Functionals. *J. Chem. Phys.* **2006**, *125*, 201102.
(108) Ruzsinszky, A.; Perdew, J. P.; Csonka, G. I.; Vydrov, O. A.; Scuseria, G. E. Density Functionals That Are One- and Two- Are Not Always Many-Electron Self-Interaction-Free, as Shown for H_2^+, He_2^+, LiH^+, and Ne_2^+. *J. Chem. Phys.* **2007**, *126*, 104102.
(109) Voora, V. K.; Balasubramani, S. G.; Furche, F. Variational Generalized Kohn-Sham Approach Combining Random Phase Approximation and Green's Function Methods, 2017, UCPMS ID: 2225536. *UCI eScholarship repository*. https://escholarship.org/uc/item/7gf3h1h9 (accessed Sept 6, 2018).
(110) Jimenez-Hoyos, C. A.; Janesko, B. G.; Scuseria, G. E. Evaluation of Range-Separated Hybrid and Other Density Functional Approaches on Test Sets Relevant for Transition Metal-Based Homogeneous Catalysts. *J. Phys. Chem. A* **2009**, *113*, 11742−11749.
(111) Jiang, W.; DeYonker, N. J.; Wilson, A. K. Multireference Character for 3d Transition-Metal-Containing Molecules. *J. Chem. Theory Comput.* **2012**, *8*, 460−468.
(112) Perdew, J. P.; Ernzerhof, M.; Burke, K. Rationale for Mixing Exact Exchange with Density Functional Approximations. *J. Chem. Phys.* **1996**, *105*, 9982.
(113) Stein, C. J.; von Burg, V.; Reiher, M. The Delicate Balance of Static and Dynamic Electron Correlation. *J. Chem. Theory Comput.* **2016**, *12*, 3764−3773.
(114) Klopper, W.; Lüthi, H. P. Towards the Accurate Computation of Properties of Transition Metal Compounds: The Binding Energy of Ferrocene. *Chem. Phys. Lett.* **1996**, *262*, 546−552.
(115) Bates, J. E.; Sengupta, N.; Sensenig, J.; Ruzsinszky, A. Adiabatic Connection without Coupling Constant Integration. *J. Chem. Theory Comput.* **2018**, *14*, 2979−2990.
(116) Kim, M.-C.; Sim, E.; Burke, K. Understanding and Reducing Errors in Density Functional Calculations. *Phys. Rev. Lett.* **2013**, *111*, 073003.

DOI: 10.1021/acs.jctc.8b00777
J. Chem. Theory Comput. 2018, 14, 5701−5714